Nanoscale

PAPER

View Article Online
View Journal | View Issue

Cite this: *Nanoscale*, 2025, **17**, 22967

Quantum dot antennas for DTE-BODIPY dyads: efficient "on–off" photoluminescence switching with a broad excitation spectrum

Phuong Thao Trinh,[a] Sina Hasenstab,[a] Karola Rück-Braun,[b] Markus Braun *[a] and Josef Wachtveitl *[a]

A dye-photoswitch dyad (consisting of BODIPY and DTE) has been studied spectroscopically. In this system, the fluorescent dye can be quenched *via* FRET by closing the photoswitch, resulting in a photomodulated fluorescence. CdSe/ZnS quantum dot (QD)/dyad complexes have been prepared to investigate the suitability of QDs as antennas to extend the excitation range of this system. Illumination experiments show that the photoswitch retains its functionality even after the dyad is attached to the QD surface. Furthermore, photoluminescence (PL) measurements show a very efficient FRET from the QD to the dyad. Transient absorption experiments reveal signals indicative of a direct FRET from the QD to the closed switch and two successive FRET processes – from the QD to the dye and subsequently from the dye to the closed switch. With this integrated spectroscopic approach, we demonstrated that QDs are well suited for enhancing photomodulated fluorescence.

Received 25th June 2025,
Accepted 18th September 2025

DOI: 10.1039/d5nr02697k

rsc.li/nanoscale

Introduction

Photochromism is the light-induced reversible conversion of a chemical species between two forms, accompanied by a change in the respective absorption spectra.[1] Molecules that undergo photochromism are also called photoswitches. Intensively studied molecules of this group are azobenzene, spiropyran and dithienylethene (DTE).[2] Azobenzene and spiropyran are classified as T-type photochromic molecules, *i.e.* their photogenerated isomers are thermally reversible. In contrast, the photogenerated isomer of DTE is thermally stable and the back reaction can only be induced photochemically, placing them in the class of P-type photochromic molecules.[3] Besides their thermal stability, DTE also provides high fatigue resistance and a conversion between a colorless open and a colored closed form due to the extended conjugation along the molecular backbone.[4] Recently, a fulgimide/dye dyad for fluorescence modulation was presented, where the thermally stable fulgimide (P-type photochromism) acts as photoswitchable quencher for dye fluorescence.[5] This dyad was successfully tested for bioimaging applications. Also, DTE photoswitches can be modified to perform thousands of isomerization events in aqueous surrounding without any significant photofatigue.[6]

Owing to these properties, DTEs are well suited as components for fluorescence modulation systems. In recent years, dyads of photochromic molecules in combination with fluorophores have been extensively studied for this purpose.[7–10] The concept of this system is based on the fact that the fluorescence of the dye (on-state) can be efficiently quenched by the closed switch (off-state) *via* electron or energy transfer.[11–13] Fluorescence on demand has enormous importance in the application areas of optical data storage,[8] photopharmacology[14] and high-resolution imaging.[15] However, the excitation range of the photomodulated fluorescence is limited by the spectrally narrow absorption of the dye.

Materials which are known for their strong and broad absorption behavior are semiconductor nanoparticles, also known as quantum dots (QDs).[16] The absorption and emission of QDs can be controlled by their composition, size and surface functionalization. Because QDs possess high fluorescence quantum yields and a narrow emission band in addition to tunable optical properties, they are often used as donors in Förster resonance energy transfer (FRET)[17] systems. The close distance between the donor and acceptor can be realized by attaching the molecule to the QD surface *via* an anchor group (*e.g.* COOH-group). Utilizing QDs as antennas not only expands the excitation range but also increases the "on"-fluorescence of the dye due to FRET. Therefore, the

[a]*Institute of Physical and Theoretical Chemistry, Goethe-Universität Frankfurt, Max-von-Laue-Str. 7, 60438 Frankfurt am Main, Germany.*
E-mail: braun@theochem.uni-frankfurt.de, wveitl@theochem.uni-frankfurt.de;
Tel: +49 (0)69 789 29711, +49 (0)69 789 29351
[b]*Institute of Chemistry, Technische Universität Berlin, Straße des 17. Juni 135, 10623 Berlin, Germany*

photomodulated fluorescence of the dye-switch systems can be further enhanced.

In this study, we investigated the energy transfer dynamics of CdSe/ZnS QDs to a BODIPY-DTE dyad. The dyad retained its photoswitching ability even after attachment to the QD. The complexes of both isomeric states were characterized by steady state and transient absorption spectroscopy. A very efficient FRET from the QD to the dyad could be determined. We will show that the attachment of the DTE-BODIPY dyad to a QD improves the fluorescence quenching efficiency of the dyad from 87% to 97%.

Experimental

Materials

Oleic acid (OA; tech. 90%), 1-octadecene (ODE; tech. 90%), trioctylphosphine (TOP; tech. 90%), cadmium oxide (99.5%), selenium (100 mesh, 99.99%), acetone (99%), toluene (99.95%) and ethanol (99.8%) were obtained from Sigma Aldrich. Methanol (100%) was obtained from Acros Organics.

Synthesis of CdSe cores

CdO (26 mg, 0.2 mmol) was dissolved in OA and ODE under argon atmosphere. This was followed by adding the Se precursor (Se (8 mg, 0.1 mmol) in 1.5 mL TOP and 0.5 mL TOP) to the Cd solution at a temperature of 205 °C. After the completed addition, the heating mantle was removed, and the reaction mixture was cooled to room temperature. The obtained QDs were washed with MeOH/EtOH (1 : 3) and then precipitated with acetone. After centrifugation, the QDs were dried under vacuum and dissolved in toluene for the subsequent experiments.

Synthesis of CdSe/ZnS core/shell QDs

First, the precursors were prepared for the synthesis of core/shell particles. The calculated amounts of the precursors should result in two monolayers of ZnS. ZnO (24 mg, 0.3 mmol) was dissolved in 2 mL OA and 2 mL ODE under an inert atmosphere. This solution was kept warm, to avoid the precipitation of ZnO. S (13 mg, 0.4 mmol) was dissolved in 0.5 mL TOP and 0.5 mL ODE.

The dried CdSe cores were dissolved in 4 mL ODE and heated to 250 °C in a three-neck flask under argon atmosphere. Then, the S solution was added. After 2 minutes, the Zn solution was injected and stirred for another 10 minutes. The reaction mixture was then cooled to room temperature. The purification procedure was analogous to that for the CdSe cores, and the CdSe/ZnS QDs were also dissolved in toluene.

The diameter of the QD was determined using the formula from Yu *et al.*[18] and was approximately 2.4 nm for the CdSe/ZnS QDs.

Preparation of QD/dyad complexes

The complexes were prepared from stock solutions of a DTE-BODIPY dyad ($\varepsilon_{531\ nm}$ = 30 000 L (mol cm)$^{-1}$ in methanol)[19] and CdSe/ZnS ($\varepsilon_{505\ nm}$ = 59 063 L (mol cm)$^{-1}$). The concentration of the QD was calculated with the extinction coefficient estimated from the empirical formula of Yu *et al.*[18] However, it must be clarified that the size-dependent extinction coefficient for CdSe/ZnS is unknown as the formula is only valid for CdSe. Nevertheless, the calculated values provide a good approximation, since the lowest excitonic peak of CdSe is well preserved.

To couple the dyad to the QD surface, we added the QD suspension in toluene to the vacuum dried dyad. The ratio of QD to dyad was set to approximately 1 : 3. The sample was mixed, placed in an ultrasonic bath for 30 min, and stored for at least 8 h (overnight) at 4 °C in an opaque vial.

Steady state spectroscopy

The absorption spectra were recorded in quartz cuvettes with an optical path length of 1 mm using an S600 spectrometer (Analytik Jena, Jena, Germany).

Photoluminescence (PL) was measured in 4 × 10 mm quartz cuvettes using an FP-8500 spectrofluorometer (Jasco, Groß-Umstadt, Germany). Baseline and wavelength-dependent instrument sensitivities were corrected. Bandwidths of 5 nm for excitation and emission were adjusted and the PMT voltage was set to 350 V. The excitation wavelength was set to 435 nm.

Time-resolved spectroscopy

The different samples were investigated by a conventional pump–probe setup described in detail elsewhere.[20] Briefly, a Clark CPA 2001 laser/amplifier system with a 775 nm fundamental wavelength, repetition rate of 1 kHz and 150 fs pulse width was used for the generation of femtosecond laser pulses. The pump pulse was converted from the fundamental wavelength and a NOPA pulse (990 nm) by a sum frequency generation, resulting in a wavelength of 435 nm. The power of the pump pulse was set to 7 nJ per pulse to prevent multiexciton generation in the measurements. White light continuum (450–650 nm) probe pulses were generated by focusing the laser fundamental into a CaF_2 crystal of 5 mm thickness. All experiments were performed under magic angle conditions (54.7° angle difference of pump–probe polarization) to eliminate anisotropic contributions. A fused silica cuvette with an optical path length of 1 mm was used. The samples were moved continuously to prevent photo-degradation.

Transient absorption data analysis

The transient absorption data were analyzed *via* global lifetime analysis (GLA) with the OPTIMUS program.[21] In GLA, all transients are simultaneously analyzed with a single set of exponential functions. The GLA results are presented as decay-associated spectra (DAS). In DAS, positive amplitudes result from either the decay of a positive or the rise of a negative absorption change, whereas negative amplitudes describe the decay of a negative or the rise of a positive absorption change.

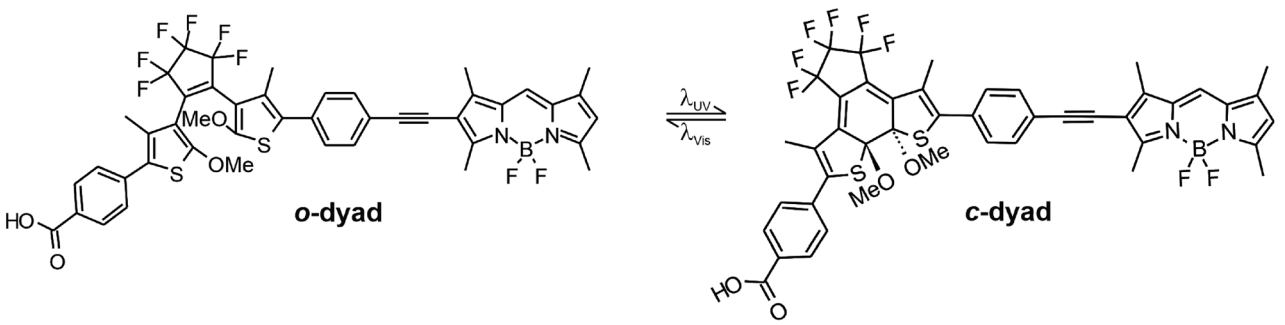

Fig. 1 Chemical structures of the DTE-BODIPY dyad in its open and closed form.

Quantum-chemical calculations

The DTE photoswitch in its open and closed form and BODIPY chromophore were investigated as separate moieties and also as complete dyad as shown in Fig. 1. All calculations were performed using the program package Gaussian 16, Revision A.03 [22] with the BHandHLYP functional and 6-311G* basis set. The electronic excitation energies as well as the ground and excited state geometries and wavefunctions were calculated by DFT and TD-DFT method for ten lowest energetic excited states. Visualization of the difference electron densities for optical transitions was carried out by the program Multiwfn.[23]

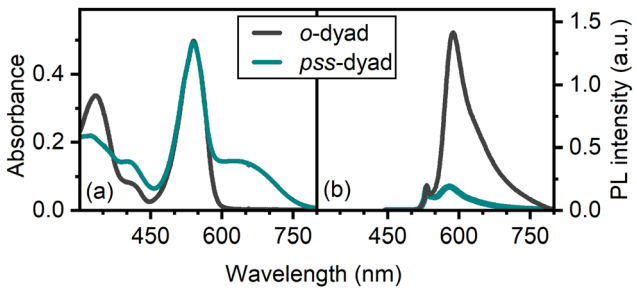

Fig. 2 (a) Absorption and (b) PL spectra (exc. 530 nm) of the dyad with DTE in its open (dark grey) and pss-state (dark cyan).

Results and discussion

Dyad – steady state characterization

The investigated dyad consists of a BODIPY which is horizontally linked to DTE through a bridging phenyl and ethinyl unit. Furthermore, a COOH-anchor group is attached to the DTE (Fig. 1).

The DTE-switch in the dyad can be converted from the open form to the closed form by a UV light induced cyclization reaction. As both, the open (o) and closed (c) form, absorb light in this range, it is usually not possible to completely convert the open isomer to the closed one. Instead, a photostationary state (pss) is established, in which the open and closed forms are in equilibrium. On the other hand, complete preparation of the open form dyad can be achieved by illumination with visible light. Depending on the state of the switch, the dyads are from now on referred to as **o-dyad** or **pss-dyad**.

The absorption spectra of **o-dyad** and **pss-dyad** are shown in Fig. 2a. The absorption band observed at 340 nm in the spectrum of **o-dyad** corresponds to the S_0–S_1 transition of o-DTE, while the band observed at 530 nm is attributed to the S_0–S_1 transition of BODIPY.[13,24] The blue-shifted shoulder, which is observed at wavelengths below 520 nm, can be attributed to the 0–1 vibronic transition.[13] Irradiation of **o-dyad** at 340 nm induces the cyclization reaction, resulting in the decrease of the 340 nm band and the formation of a new band around 650 nm. The conjugated π-system is enlarged as the ring closes, causing a significant red-shift in the absorption of the switch. Therefore, the broad absorption band observed between 450–760 nm can be attributed to the S_0–S_1 transition of c-DTE.[24] The closed form can be converted to the open form by irradiation at 625 nm.

Instead of methyl groups, methoxy groups function as substituents at the C2 and C2′ positions of DTE in the dyad. The transition from o-DTE to c-DTE and *vice versa* occurs ultrafast *via* a conical intersection. However, for the cycloreversion, a barrier must first be overcome before reaching the conical intersection.[3,25–28] The energetic position of this barrier is significantly influenced by the substituents at the reactive carbons.[29] In this case, the methoxy groups increase this barrier and drastically reduce the quantum yield of the cycloreversion. As a result, quantitative switching of both states (excitation at 340 nm for the ring closing and at 625 nm for the ring opening reaction) can occur (ratio o : c in $pss_{340\ nm}$ was determined to be 0 : 100 by HPLC).[30]

The photochromic class of DTE photoswitches is known for thermally stable ground-state isomers and high fatigue resistance.[4] While the photochemical fatigue of the dyad was not investigated systematically in this work, it can be stated that after five complete isomerization cycles, the steady-state optical spectra and the transient absorption signals of the samples were unchanged and no indications of degradation were observed.

The PL measurement of **o-dyad** shows a strong emission with a maximum at 580 nm, which can be attributed to the emission of BODIPY. After the isomerisation reaction, a signifi-

cant reduction of the emission intensity can be observed. Due to the strong redshift of the c-DTE absorption of the closed isomer, it overlaps with the emission of BODIPY. This enables FRET from BODIPY to c-DTE, resulting in a quenched dye emission. The strong quenching (87%) indicates a particularly efficient FRET process. In this way, the fluorescence of BODIPY can be controlled by photoinduced switching of the DTE moiety and thus enables a photomodulated fluorescence.

Dyad – quantum chemical calculation

For the dyad vertical excitation energies were calculated by the TD-DFT method with the DTE moiety in the open or closed state. The obtained parameters for the lowest optical transitions are summarized in Table 1 and the corresponding difference electron densities are visualized in Table 2. It can be seen that the values of transition 1 and 2 for the dyad with open DTE are nearly identical to the values of transition 2 and 4 for the dyad with closed DTE. The difference electron density plot shows that these transitions are perfectly localized on the BODIPY moiety in the respective dyad. The high energetic transition 3 of the dyad with o-DTE is strongly localized on the DTE moiety and also transitions 1 and 3 of the dyad with c-DTE are localized on the DTE part of the dyad. The corresponding values for transition energy E and oscillator strength f are similar to results for an isolated DTE switch in the open state (4.2362 eV [292.68 nm] f = 0.5836) or closed state (2.4579 eV [504.44 nm] f = 0.3394 and 3.6687 eV [337.95 nm] f = 0.1597). This finding allows the interpretation that the electronic coupling of BODIPY and DTE is weak and that energy transfer between these moieties can be treated similarly to FRET between isolated chromophores.

Dyad – transient absorption

Initially, the dyads were investigated by direct excitation (at 520 nm) of the BODIPY chromophore (Fig. 3). For **o-dyad** (Fig. 3, top, left) a ground-state bleach (GSB) signal at approximately 530 nm was observed, which extends into the nanosecond range. In addition to the GSB signal, another strong negative signal was detected at about 540 nm, which decayed after about 1 ps. Concurrently with the decay of this signal, another spectrally broad negative signal appeared at around 650 nm. Both of these signals can be attributed to the stimulated emission (SE) based on their spectral position. The change in the spectral signature from 1 ps to 5 ps can be attributed to the spectral red-shift of the SE. Additionally, an excited-state absorption (ESA) was observed at 470 nm.

In **pss-dyad** (Fig. 3, bottom, left) the negative signature around 530 nm is spectrally narrower and shorter-lived than in **o-dyad**. This can be attributed to the absence of the SE and the partial overlap with a broad ESA of the c-DTE (<500 nm), resulting in a narrower spectral band at 530 nm. After excitation, energy is transferred to c-DTE, leading to the recovery of the BODIPY GSB at 530 nm and the decay of the BODIPY ESA at 470 nm within a few hundred femtoseconds.

To gain insight into the dynamics, we analyzed the transient data obtained from global lifetime analysis (GLA) which led to decay associated spectra (DAS, Fig. 3, right side). The **o-dyad** (Fig. 3, top, right) required four lifetimes to adequately describe the dynamics observed in the transient data. The spectrum of the first lifetime of 0.4 ps is dominated by a strong redshift of the SE signal, accompanied by minor changes in the ESA signal (<500 nm). For the second lifetime of 2.7 ps a further redshift of the SE signal can be observed. Both lifetimes can thus be correlated with fast relaxation processes in the excited state. This could indicate either motion out of the Franck–Condon region or the transition to a lower energy state. A third very weak DAS component was obtained for a lifetime of 61 ps and showed a sigmoidal spectral signature which is typical for cooling processes. Finally, the fourth time constant of 1.2 ns accounted for the decay of all signals and reflected the relaxation of the excited BODIPY to the ground state.

For the DAS of the **pss-dyad** (Fig. 3, bottom, right) the first time constant of 0.1 ps represents the recovery of BODIPY-GSB (at 530 nm) and the emergence of c-DTE-ESA signals <500 nm and >600 nm. The simultaneous decay and emergence of these signals indicate a rapid energy transfer from BODIPY to c-DTE. The decay of all signals and the subsequent relaxation of c-DTE to the ground state occurs at 1.4 ps. A derivative-like signature is observed for the third lifetime of 23 ps, which has been attributed to a ground-state cooling process in similar systems. The low quantum yield of the cycloreversion reaction of the dimethoxy substituted DTE moiety used in our study also prevents DTE isomerization.[30] The long lifetime of 2.4 ns likely describes a weak residual decay of BODIPY.

In principle, it was shown that the dyad examined is very well suitable for fluorescence modulation. However, the system could be further optimized with the help of a QD.

QD/dyad complex

For an efficient FRET within the QD-dyad systems, various conditions must be met. Since a point dipole is assumed for (nearly) spherical QDs (Fig. S1) and the binding geometry of QD and dyad is not known, the orientation of the transition dipole moments is neglected here.[31] The required short

Table 1 Vertical excitation energies E (wavelength) and corresponding oscillator strength f

Dyad with open DTE switch			Dyad with closed DTE switch			
No.	Energy/eV [nm]	f	No.	Energy/eV [nm]	f	Transition localized on
	—	—	1	2.4003 [516.53]	0.7024	DTE (closed state)
1	2.8700 [432.00]	1.1683	2	2.8819 [430.22]	0.9970	BODIPY
	—	—	3	3.5611 [348.16]	0.2480	DTE (closed state)
2	3.6854 [336.42]	0.1160	4	3.6874 [336.24]	0.1667	BODIPY
3	4.0917 [303.01]	1.2480		—	—	DTE (open state)

Table 2 Visualization of the lowest excited states of the dyad with open or closed DTE switch

Dyad with open DTE switch		Dyad with closed DTE switch		
No.		No.		Transition localized on
1	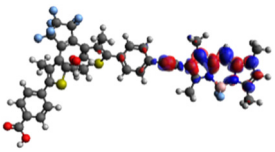	1	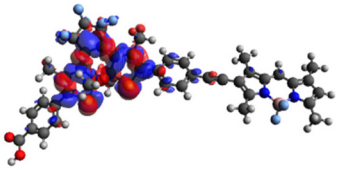	DTE (closed state)
2	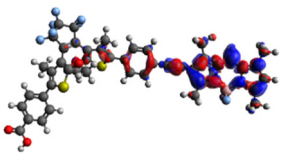	2	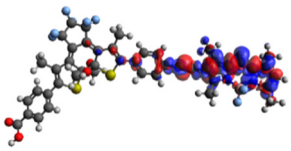	BODIPY
3	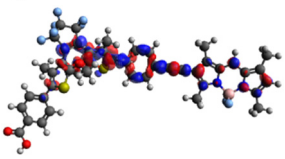	3	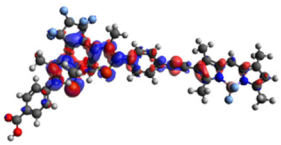	DTE (closed state)
		4	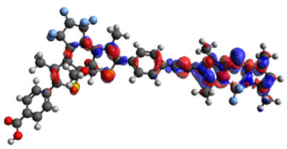	BODIPY
				DTE (open state)

The difference electron density is calculated upon excitation from the electronic ground state to the corresponding excited state.

donor–acceptor distance (Table S1) is already provided by the attachment of the dyad to the QD surface. However, the QD emission must overlap spectrally with the absorption of the dye and competing processes must be suppressed. QDs are particularly suitable to serve as antenna material since their absorption and emission maxima depend on their size and composition. Thus, they can be optimized for the respective acceptor. Often core/shell particles are used as FRET donors regarding their improved properties.[32] Here, CdSe is used as the core material and ZnS as the shell material. Due to the energetic position of the valence and conduction bands, this type I QD hinders a possible electron transfer to the acceptor (Fig. S2) and shows an enhanced photostability and fluorescence quantum yield. The anchor group of the dyad with the phenyl spacer together with the ZnS shell of the QD prevent charge transfer reactions between QD and chromophore,[33] therefore energy transfer occurs here *via* the FRET process.

The CdSe/ZnS QD shows a relatively clear absorption peak for the lowest excitonic transition at 504 nm. As common for QDs, the absorption is strong and broad at lower wavelengths. Therefore, excitation could occur far beyond the BODIPY absorption with CdSe/ZnS as an antenna. The narrow PL band at 525 nm provides the possibility of selective and efficient excited state transfer to the acceptor due to a good overlap of QD emission and BODIPY absorption (Fig. S3).

The absorption characteristics of the coupled system (Fig. 4a) results from the scaled addition of the **QD** and the dyad spectra (Fig. S4). The most important prerequisite is that the dyad can still function normally in the coupled system. Fig. S5 shows the irradiation experiment from **QD**/**o-dyad** to **QD**/**pss-dyad** and *vice versa*. The ring closing and opening reactions can each be optically induced in the same way as for the pure dyads. After several photochemical conversion experiments of the coupled QD-dyad system the optical spectra of the samples were unchanged and no indications of degradation were observed.

PL spectra of the **QD**/**o-dyad** complex (Fig. 4b) show a decrease of the QD emission band and simultaneously an increase of the BODIPY emission after excitation at 435 nm (minimum of dyad absorption to avoid direct excitation). It is possible to scale the PL of **o-dyad** to the PL spectra of the complex at higher wavelengths. Subsequent subtraction leads to the PL spectra of the pure **QD** (Fig. S6). Thus, it can be reasonably concluded that the PL of the QD is quenched by 82% and that of the **o-dyad** increases. Excitation of the **QD**/

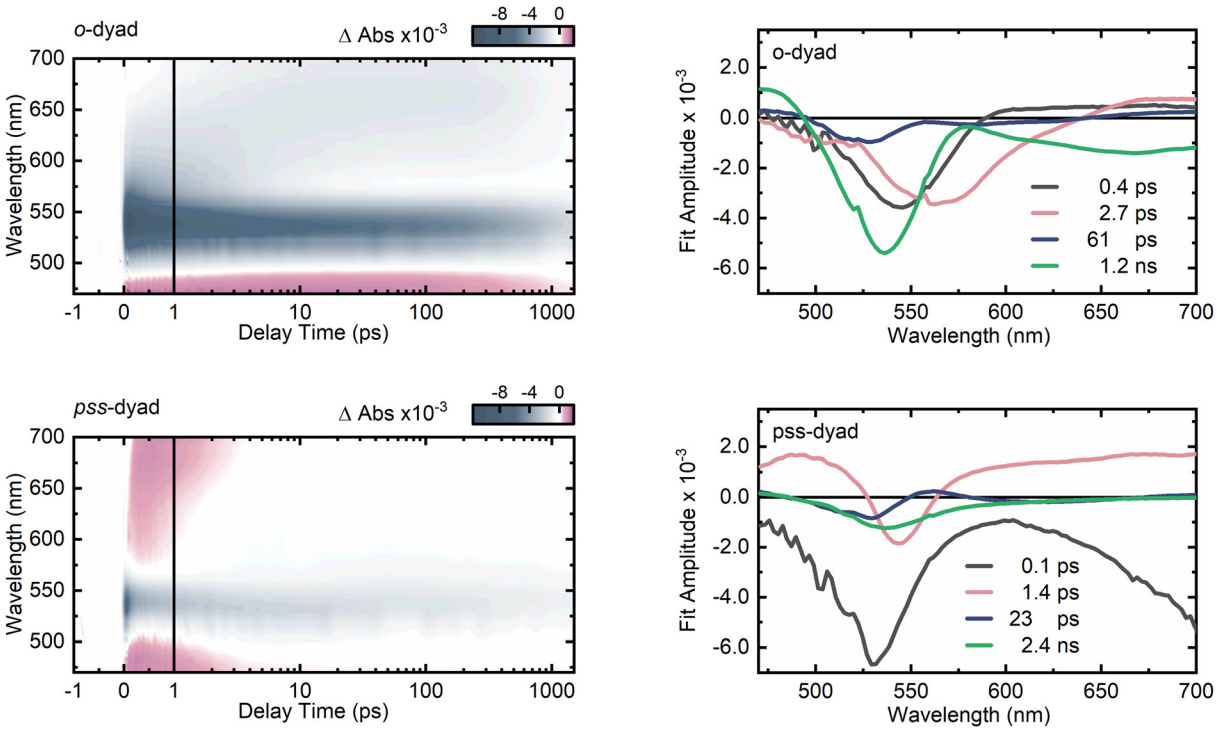

Fig. 3 Transient absorption map of **o-dyad** (top, left) and **pss-dyad** (bottom, left) after excitation at 520 nm. The respective decay-associated spectra (DAS) of **o-dyad** (top, right) and **pss-dyad** (bottom, right) are obtained with four decay components.

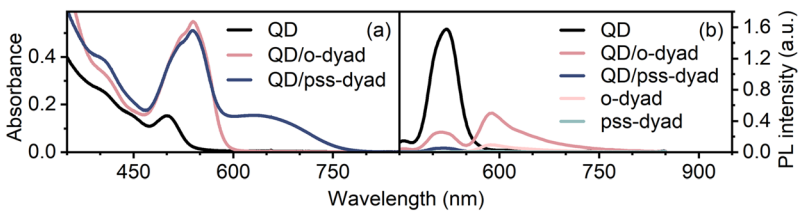

Fig. 4 (a) Absorption and (b) PL spectra (exc. 435 nm) of the **QD** (black), **QD/o-dyad** (pink), **QD/pss-dyad** (blue), **o-dyad** (light pink) and **pss-dyad** (light blue).

pss-dyad complex leads to an even stronger quenching of the QD PL by 98% (Fig. 4b). The dyad PL (which just results from the BODIPY since DTE has a very low fluorescence QY) is completely quenched indicating a subsequent FRET from BODIPY to c-DTE. However, the isomeric state of the DTE shouldn't influence the FRET from QD to BODIPY, assuming a subsequent FRET. The enhanced quenching for **QD/pss-dyad** points to another process taking place. Since the c-DTE absorption is very broad, it also overlaps with the QD PL. Therefore, a direct FRET from QD to c-DTE is also possible and would further reduce the QD PL.

Energy transfer

Femtosecond transient absorption (TA) measurements at an excitation wavelength of 435 nm were performed to investigate the ultrafast processes of the new systems. The absorption of the pure dyads is minimal at this pump wavelength (Fig. S7) while the QDs are strong absorbers in this spectral range.

The pure **QD** (Fig. 5, top, left) shows a strong GSB signal around the lowest excitonic transition at 505 nm. This signal is caused by the state filling effect and strongly overlaps with the stimulated emission (SE) around 525 nm. Both signals (GSB and SE) show long lifetimes (>1.2 ns – the measurement window) and thus indicate a slow recombination. Furthermore, two positive signals can be observed in the TA map. One is a short-lived signal at ~540 nm, resulting from the Stark effect.[34,35] The other is a broad signal >550 nm, which has previously been assigned to intra-band transitions of the hole.[36,37] *Via* GLA (Fig. 5, top, right) a time constant of 4.1 ns was determined for the charge carrier recombination within the QD as it shows the decay of all signals. A short lifetime of 0.4 ps can be assigned to the decay of the Stark effect. The very weak signal component with lifetime of 25 ps most

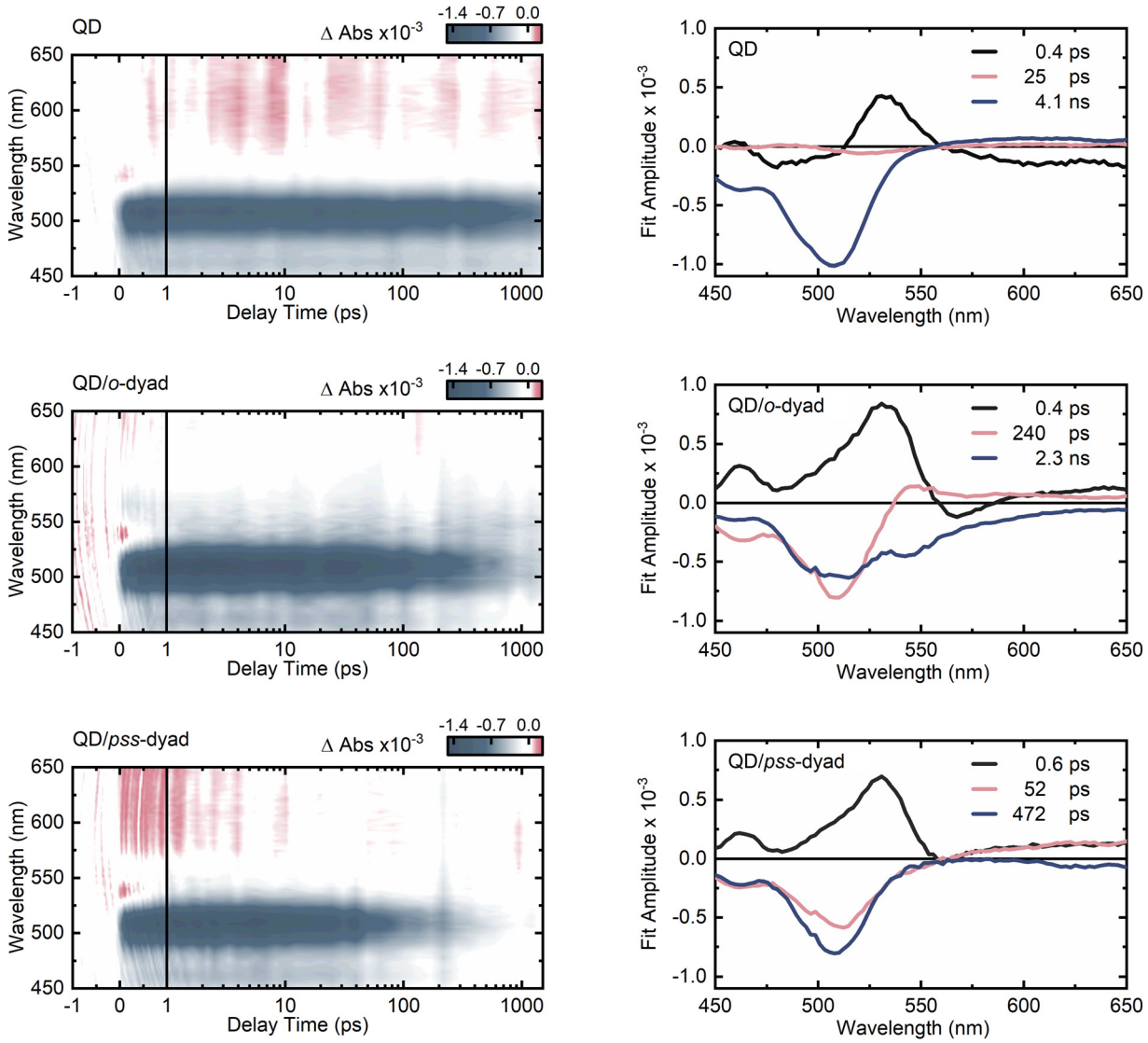

Fig. 5 Transient absorption map of the **QD** (top, left), the **QD/o-dyad** (middle, left) and the **QD/pss-dyad** (bottom, left) after excitation at 435 nm. The respective decay-associated spectra (DAS) of the **QD** (top, right), the **QD/o-dyad** (middle, right) and the **QD/pss-dyad** (bottom, right) are obtained with three decay components.

likely describes minor intrinsic relaxation processes related to trap states.[38]

In Fig. 5 (middle row and bottom row) also the transient absorption data of the complexes is depicted. While, the pure **QD** sample shows a very long lived GSB, the decay of the long-lived GSB signal of the QD is accelerated in the hybrid systems. This acceleration is most pronounced for the complex with the **pss-dyad** (Fig. 5, bottom, left). This is in agreement with the PL data, where the quenching of the QD PL is increased for the **QD/pss-dyad**. As mentioned above, a direct FRET from QD to c-DTE could be a possible explanation.

To further analyze this data, all TA datasets were fitted using global lifetime analysis (GLA). Three lifetime components were sufficient for a satisfactory fit of the data. The resulting amplitude spectra of each lifetime are depicted in the decay associated spectra (Fig. 5, right side). The first lifetime component (0.4 ps and 0.6 ps, respectively) reflects the decay of the Stark effect signal for both samples. For **QD/o-dyad** (Fig. 5, middle, right) the second lifetime (240 ps) is characterized by the decay of the QD bleach, as well as the formation of the BODIPY GSB and SE. For **QD/pss-dyad** (Fig. 5, bottom, right) the spectral signature of the second lifetime (52 ps) differs at longer wavelengths. Instead of the formation of the BODIPY GSB at ~540 nm, a decay of the latter is observed, which is accompanied by the formation of the c-DTE GSB in the range from 600–650 nm. Thus, the second lifetime in the complexes represents the FRET from QD to BODIPY. In the case of **QD/pss-dyad**, the subsequent FRET from BODIPY to c-DTE appears to proceed so rapidly that both FRET processes are occurring simultaneously. On the other hand, a con-

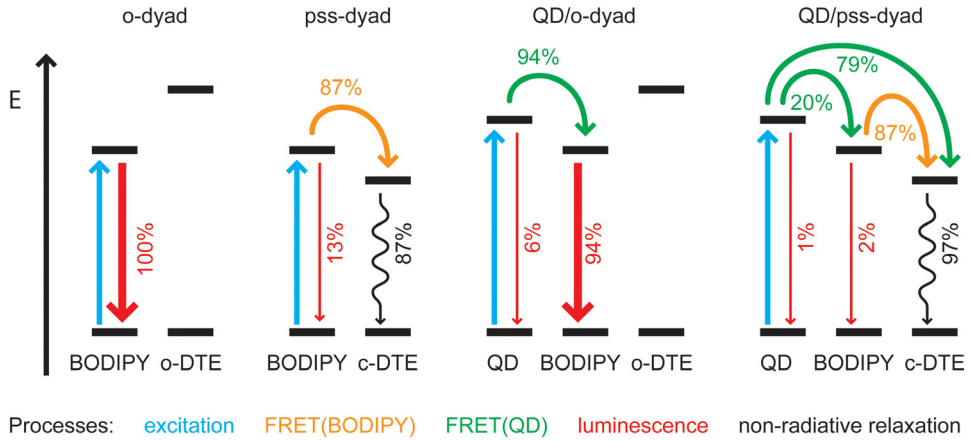

Fig. 6 Schematic presentation of the occurring processes in the QD/dyad complexes after excitation of the QD. In the system **QD/pss-dyad** 79% of the QD excited state population is transferred directly to c-DTE and 20% is transferred to BODIPY. By a subsequent FRET process 87% of these 20% (= 18%) are transferred to c-DTE.

tribution could also be due to the direct FRET from QD to c-DTE. The recombination process of the final acceptor can be assigned to the last lifetime component. For **QD/o-dyad** an additional relaxation process of the previously excited BODIPY can be observed. **QD/pss-dyad** on the other hand shows the relaxation process of c-DTE.

Starting from an excited state of the system, several processes can take place until the system returns to the ground state. The lifetimes determined from the GLA are used for further analysis to quantify the individual processes. Furthermore, following equations were needed:

$$k_n = \frac{1}{\tau_n}.$$

The excited state lifetime for the pure QD is 4.1 ns, which means that the recombination rate is k_1 = 0.24 ns^{-1}. In the coupled system with o-dyad, the lifetime of the excited state is reduced to 240 ps because an additional deactivation pathway is added. Assuming that only recombination and FRET take place in this system, the FRET rate from QD to BODIPY can be calculated as follows:

$$k_{\mathrm{FRET}_1} = k_2 - k_1$$

with k_2 = (1/240 ps) = 4.17 ns^{-1} the rate for FRET is k_{FRET_1} = 3.92 ns^{-1}.

For the complex with **pss-dyad** there are even three processes possible: recombination, FRET from QD to BODIPY and a direct FRET from QD to c-DTE. This of course further reduces the lifetime of the excited state to 52 ps.

$$k_{\mathrm{FRET}_2} = k_3 - k_{\mathrm{FRET}_1} - k_1$$

With k_3 = 1/(52 ps) = 19.23 ns^{-1} the rate for FRET from QD to c-DTE is k_{FRET_2} = 15.15 ns^{-1}.

The obtained rates can be used to calculate the percentage distribution of each process in each system assuming that only the recombination and FRET processes take place. The results are summarized in Fig. 6. For the **QD/o-dyad**, 94% of the relaxation rate is due to the FRET process from QD to BODIPY. However, for the steady state fluorescence the observed quenching of the QD was only 82%. This small deviation can be explained by the fact, that not all QDs have the same amount of dyad attached to the surface. Considering a Poisson distribution of dyads per QD, there are also QDs with no acceptor at all and therefore these QDs have no quenched PL. This can also be seen in the DAS since there is still a residual QD GSB decay of those QDs without a dyad attached. This explains why the quenching in the fluorescence data was not as high as expected.

For **QD/pss-dyad** FRET_1 takes place at 20% and FRET_2 at 79%. The high favorability of FRET_2 can be explained by the higher FRET rate and also the shorter donor acceptor distance (Table S1). Taking both FRET pathways into account, this should lead to a total QD quenching of 99%. The steady state fluorescence data with a 98% quenching fits well to this result. Small deviations can again be explained by the non-uniform acceptor distribution.

Conclusion

A dyad consisting of a dye and switch was characterized *via* steady state fluorescence and transient absorption measurements. The measurements showed an efficient on/off-switching of the BODIPY fluorescence due to an ultrafast FRET. Therefore, this dyad proved to be suitable for photomodulated fluorescence.

The presented QD/dyad complex was investigated in the context of enhanced photomodulated fluorescence. The complex retained its switching ability even after attachment to the QD surface. Thus, this functionality of the dyads can still be provided – with the addition of further benefits. The QD antenna significantly broadens the excitation range of the photomodulated fluorescence and increases the "on"-fluorescence. Furthermore, the complex with the closed dyad shows even higher PL quenching, since additionally to the

FRET from QD to BODIPY to c-DTE also the direct FRET from QD to c-DTE takes place. Due to the close donor–acceptor distance the direct FRET is even more favorable (79% direct FRET). The additional relaxation pathway does not affect the validity of this approach, since the goal is to quench the fluorescence as much as possible, which is certainly achieved with an additional quenching mechanism.

Overall, the investigated QD/dyad system exhibits excellent and expanded properties for potential utilization of antenna supported systems in photomodulated fluorescence applications.

Conflicts of interest

There is no conflict of interests.

Data availability

The data supporting this article have been included as part of the SI. Data for this article, including spectroscopic data, input geometries and LVC parameters will be available at GUDE (Goethe University Data Repository) at **https://gude.uni-frankfurt.de/workflowitems/301/view**. All data presented will be made available upon reasonable request.

Supplementary information is available. See DOI: **https://doi.org/10.1039/d5nr02697k**.

Acknowledgements

Generous support by the German Research Foundation (K. R.-B.: DFG, SFB 658, B6; and J. W.: DFG, grant WA 1850/6-2, WA 1850/11-1 and GRK 1986) is gratefully acknowledged.

The authors gratefully acknowledge Nandor Ziebart (Rück-Braun group; TU Berlin) for the synthesis and HPLC measurements of the dyad.

References

1 H. Bouas-Laurent and H. Dürr, *Pure Appl. Chem.*, 2001, **73**, 639–665.
2 A. Gonzalez, E. S. Kengmana, M. V. Fonseca and G. G. D. Han, *Mater. Today Adv.*, 2020, **6**, 21.
3 M. Irie, T. Fukaminato, K. Matsuda and S. Kobatake, *Chem. Rev.*, 2014, **114**, 12174–12277.
4 M. Irie, *Chem. Rev.*, 2000, **100**, 1685–1716.
5 K. Torii, Y. Hori and K. Kikuchi, *Anal. Chem.*, 2023, **95**, 8834–8841.
6 K. Uno, M. L. Bossi, M. Irie, V. N. Belov and S. W. Hell, *J. Am. Chem. Soc.*, 2019, **141**, 16471–16478.
7 A. Fihey and D. Jacquemin, *Chem. Sci.*, 2015, **6**, 3495–3504.
8 N. H. Xie, C. Fan, H. Ye, K. Xiong, C. Li and M. Q. Zhu, *ACS Appl. Mater. Interfaces*, 2019, **11**, 23750–23756.
9 Z. Y. Li, M. N. Li, G. X. Liu, Y. Y. Wang, G. H. Kang, C. Y. Li and H. Guo, *Dyes Pigm.*, 2019, **160**, 597–603.
10 Q. Yan, Z. Qiao, J. Y. Xu, J. Ren and S. Wang, *Dyes Pigm.*, 2022, **202**, 7.
11 F. M. Raymo and M. Tomasulo, *Chem. Soc. Rev.*, 2005, **34**, 327–336.
12 J. Cusido, E. Deniz and F. M. Raymo, *Eur. J. Org. Chem.*, 2009, 2031–2045.
13 F. Schweighöfer, I. Yüce, L. Dworak, P. Guo, M. Zastrow, K. Mayer, C. Barta, D. Liebmann, N. Ziebart, K. Rück-Braun and J. Wachtveitl, *J. Phys.: Condens. Matter*, 2018, **30**, 7.
14 H. N. Zhang, X. X. Hu, H. J. Zhu, L. M. Shen, C. M. Liu, X. M. Zhang, X. Y. Gao, L. M. Li, Y. P. Zhu and Z. Y. Li, *Front. Chem.*, 2021, **9**, 10.
15 C. Benitez-Martin, S. M. Li, A. Dominguez-Alfaro, F. Najera, E. Pérez-Inestrosa, U. Pischel and J. Andréasson, *J. Am. Chem. Soc.*, 2020, **142**, 14854–14858.
16 M. A. Reed, J. N. Randall, R. J. Aggarwal, R. J. Matyi, T. M. Moore and A. E. Wetsel, *Phys. Rev. Lett.*, 1988, **60**, 535–537.
17 T. Förster, *Discuss. Faraday Soc.*, 1959, 7–17.
18 W. W. Yu, L. H. Qu, W. Z. Guo and X. G. Peng, *Chem. Mater.*, 2003, **15**, 2854–2860.
19 N. Ziebart, F. Schröder and K. Rück-Braun, *ChemPhotoChem*, 2019, **3**, 396–402.
20 J. Helbing, H. Bregy, J. Bredenbeck, R. Pfister, P. Hamm, R. Huber, J. Wachtveitl, L. De Vico and M. Olivucci, *J. Am. Chem. Soc.*, 2004, **126**, 8823–8834.
21 C. Slavov, H. Hartmann and J. Wachtveitl, *Anal. Chem.*, 2015, **87**, 2328–2336.
22 M. J. Frisch, G. W. Trucks, H. B. Schlegel, G. E. Scuseria, M. A. Robb, J. R. Cheeseman, G. Scalmani, V. Barone, G. A. Petersson, H. Nakatsuji, X. Li, M. Caricato, A. V. Marenich, J. Bloino, B. G. Janesko, R. Gomperts, B. Mennucci, H. P. Hratchian, J. V. Ortiz, A. F. Izmaylov, J. L. Sonnenberg, D. Williams-Young, F. Ding, F. Lipparini, F. Egidi, J. Goings, B. Peng, A. Petrone, T. Henderson, D. Ranasinghe, V. G. Zakrzewski, J. Gao, N. Rega, G. Zheng, W. Liang, M. Hada, M. Ehara, K. Toyota, R. Fukuda, J. Hasegawa, M. Ishida, T. Nakajima, Y. Honda, O. Kitao, H. Nakai, T. Vreven, K. Throssell, J. A. Montgomery Jr., J. E. Peralta, F. Ogliaro, M. J. Bearpark, J. J. Heyd, E. N. Brothers, K. N. Kudin, V. N. Staroverov, T. A. Keith, R. Kobayashi, J. Normand, K. Raghavachari, A. P. Rendell, J. C. Burant, S. S. Iyengar, J. Tomasi, M. Cossi, J. M. Millam, M. Klene, C. Adamo, R. Cammi, J. W. Ochterski, R. L. Martin, K. Morokuma, O. Farkas, J. B. Foresman and D. J. Fox, *Gaussian 16*, Revision A.03, Gaussian, Inc., Wallingford CT, 2016.
23 T. Lu and F. W. Chen, *J. Comput. Chem.*, 2012, **33**, 580–592.
24 J. Ern, A. T. Bens, A. Bock, H. D. Martin and C. Kryschi, *J. Lumin.*, 1998, **76–7**, 90–94.
25 Y. Asano, A. Murakami, T. Kobayashi, A. Goldberg, D. Guillaumont, S. Yabushita, M. Irie and S. Nakamura, *J. Am. Chem. Soc.*, 2004, **126**, 12112–12120.
26 M. Boggio-Pasqua, M. Ravaglia, M. J. Bearpark, M. Garavelli and M. A. Robb, *J. Phys. Chem. A*, 2003, **107**, 11139–11152.

27 D. Guillaumont, T. Kobayashi, K. Kanda, H. Miyasaka, K. Uchida, S. Kobatake, K. Shibata, S. Nakamura and M. Irie, *J. Phys. Chem. A*, 2002, **106**, 7222–7227.
28 K. Uchida, D. Guillaumont, E. Tsuchida, G. Mochizuki, M. Irie, A. Murakami and S. Nakamura, *J. Mol. Struct.: THEOCHEM*, 2002, **579**, 115–120.
29 S. Nakamura, T. Kobayashi, A. Takata, K. Uchida, Y. Asano, A. Murakami, A. Goldberg, D. Guillaumont, S. Yokojima, S. Kobatake and M. Irie, *J. Phys. Org. Chem.*, 2007, **20**, 821–829.
30 N. Ziebart, P. Schroeer and K. Rueck-Braun, *Tetrahedron*, 2018, **74**, 5561–5566.
31 I. L. Medintz and H. Mattoussi, *Phys. Chem. Chem. Phys.*, 2009, **11**, 17–45.
32 S. Roth, P. T. Trinh and J. Wachtveitl, *Nanoscale*, 2021, **13**, 9808–9815.
33 R. Singh, S. Akhil, V. G. V. Dutt and N. Mishra, *Inorg. Chem.*, 2022, **61**, 1059–1066.
34 V. Klimov, S. Hunsche and H. Kurz, *Phys. Rev. B: Condens. Matter Mater. Phys.*, 1994, **50**, 8110–8113.
35 V. I. Klimov, *J. Phys. Chem. B*, 2000, **104**, 6112–6123.
36 J. E. Huang, Z. Q. Huang, S. Y. Jin and T. Q. Lian, *J. Phys. Chem. C*, 2008, **112**, 19734–19738.
37 A. J. Morris-Cohen, M. T. Frederick, L. C. Cass and E. A. Weiss, *J. Am. Chem. Soc.*, 2011, **133**, 10146–10154.
38 C. Giansante and I. Infante, *J. Phys. Chem. Lett.*, 2017, **8**, 5209–5215.